DASHUANG LIU◉[1,2,3*], YUCHENG WU◉[1], WEIMIN LONG◉[2,4], PING WEI◉[3],
RUI WANG◉[3], WEI ZHOU◉[1,5]

ACIDIC CORROSION BEHAVIOUR OF NIOBIUM-ADDED WELDING OVERLAYS FABRICATED BY SELF-SHIELDED METAL-CORED WIRES

Both corrosion and abrasion remove materials from some engineering components such as impact coal crusher hammers, pulverizer rings, chute liner, and rolls or molds. Intensive research has been done on improving the wear resistance of high chromium alloys, however, studies into corrosion resistance of high chromium alloys are insufficient. In order to determine the amount of ferroniobium addition in the wire to achieve the best corrosion resistance, and find out the mechanism of ferroniobium enhancing the corrosion resistance of the welding overlays, the high-Cr iron-based welding overlays with different niobium addition were fabricated by using self-made self-shielded metal-cored wires and their acidic corrosion resistance in 3.5 wt.% NaCl solution + 0.01 mol/L HCl solution were investigated by electrochemical corrosion test. The microstructure and corrosion morphology were characterized by OM, SEM, XRD and EDS. The polarization curves and values of I_{corr}, E_{corr} and R_c indicate the corrosion resistance is at the highest with 3.6 wt.% niobium addition, and at the lowest when the niobium addition is 10.8 wt.%. The corrosion of welding overlay occurs in the matrix of microstructure. With the increase of niobium addition from 3.6 wt.% to 10.8 wt.%, the proportion of network eutectic structure in the welding overlay is increased. Up to 10.8 wt.%, the microstructure is transformed from hypereutectic structure into eutectic one, leading to a higher acceleration of corrosion rate. When niobium addition reaches 14.4 wt.%, the welding overlay is transformed into a hypoeutectic structure. The addition of niobium element consumes carbon element in the alloy, which makes the increase of chromium content in the final solidified matrix, leading to an improvement in corrosion resistance.

Keywords: acidic corrosion behavior; niobium addition; self-shielded metal-cored wire

1. Introduction

Both corrosion and abrasion remove materials from some engineering components such as impact coal crusher hammers, pulverizer rings, chute liner, and rolls or molds [1-7]. High-Cr iron-based alloys have excellent wear resistance which results primarily from the presence of high volume fraction of very hard chromium carbides in a strong supporting matrix within the microstructure [2-4]. Moreover, the higher alloy content especially chromium can significantly improve the corrosion resistance of high-Cr iron-based alloys to corrosive conditions, such as reducing acids [8,9]. The corrosion resistance of these high chromium alloys largely depended on the Cr concentrations in the matrix and the volume fraction of carbides [10]. It has been reported by Ref [11]. that in the anodic polarization tests a passive film can form faster in the 27 wt.% Cr high chromium cast iron than in the 20 wt.% Cr high chromium cast iron, and the ferritic matrix in 36 wt.%Cr high chromium cast iron was the most corrosion resistant in that it exhibited a wider passive range and lower current density than the pearlitic or austenitic/martensitic matrices in 20 wt.% Cr and 27 wt.% Cr high chromium cast irons. However, the intergranular corrosion of high-Cr iron-based alloys easily takes place in a strong acidic medium because the free corrosive potential difference between carbide and matrix is the driving force of the inter-phase corrosion [9].

The change in volume fraction of the primary and eutectic carbides and refinement of primary carbide influenced the corrosion behavior of the hardfacing alloys [12]. It was demonstrated that the austenitic structured materials (for stainless steels and white cast irons) suffered lower overall material loss compared

[1] HEFEI UNIVERSITY OF TECHNOLOGY, SCHOOL OF MATERIAL SCIENCE AND ENGINEERING, HEFEI 230009, CHINA
[2] ZHENGZHOU RESEARCH INSTITUTE OF MECHANICAL ENGINEERING CO., LTD., ZHENGZHOU 450001, CHINA
[3] JIANGSU UNIVERSITY OF SCIENCE AND TECHNOLOGY, SCHOOL OF MATERIAL SCIENCE AND ENGINEERING, ZHENJIANG 212003, CHINA
[4] CHINA INNOVATION ACADEMY OF INTELLIGENT EQUIPMENT (NINGBO) CO.,LTD, NINGBO 315700, CHINA
[5] SCHOOL OF MECHANICAL AND AEROSPACE ENGINEERING, NANYANG TECHNOLOGICAL UNIVERSITY, 50 NANYANG AVENUE, 639798, SINGAPORE

* Corresponding author: dsliu@hfut.edu.cn

with the martensitic structured materials in the acidic conditions [13]. Therefore, the microstructure of high-Cr iron-based alloys play a key role in their corrosion resistance. The final state of microstructure mainly depends on the chemical composition of high-Cr iron-based alloys [14-15]. Since niobium is an important strengthening and modifying element in alloys, the previous research focused on that Nb was added into the high-Cr iron-based alloys to change their microstructure remarkably and thus improve the wear resistance [15-19]. However, there are very few works investigating how to influence the corrosion resistance by niobium addition in the high-Cr iron-based alloys. There are two objectives of the present work: one is to determine the content of ferroniobium added in the wire that contributes to the best corrosion resistance, and the other is to find out the influence mechanism of ferroniobium on the corrosion resistance of welding overlays. Therefore, we fabricated high-Cr iron-based alloys with different niobium addition by using self-made self-shielded metal-cored wires and investigated their microstructure and corrosion resistance.

2. Experimental procedures

The method of making the self-shielded metal-cored wire comprised the steps of forming a composite wire by deforming a low carbon steel strip having a flux into a sheath enclosing a core wire and then reducing the diameter of the composite wire. The chemical composition of the low carbon steel strip was $C \leq 0.10$ wt.%, $Si \leq 0.03$ wt.%, Mn: 0.30-0.55 wt.%, $P \leq 0.030$ wt.%, $S \leq 0.030$ wt.%. The flux contained ferroniobium, high carbon ferrochrome, ferroboron, electrolytic ferrosilicon, manganese, graphite and iron. Fig. 1 shows flow chart for manufacture of metal-cored wires. A flux filling rate of the wire was 55%. Different additions of Fe-Nb (containing 60 wt.% Nb) adding into core wire was 6 wt.%, 12 wt.%, 18 wt.%, and 24 wt.%, which means the addition of added niobium was 3.6 wt.%, 7.2 wt.%, 10.8 wt.% and 14.4 wt.%, respectively. The balance was made up of iron powders. The diameter of the final wire was 2.4 mm.
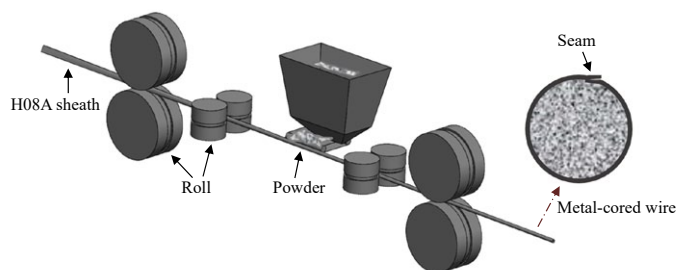

Fig. 1. Flow chart for manufacture of metal-cored wires

The consumables used were self-shielded metal-cored wires. Mild steel with the dimensions of $50 \times 70 \times 150$ mm was the substrate and five layers were deposited on its surface for each specimen. The welding parameters: welding current 280-340 A, arc voltage 28-32 V, welding speed 2.5-3.0 m·min^{-1}, electrode angle to plate surface 10° and electrode polarity of positive.

The top surface of metallographic samples was suitably sectioned after the deposition process and polished using standard metallographic techniques. The polished samples were etched using the agent (15 mL of 38% hydrochloric acid solution, 50 mL H_2O, 3 mL of 68% nitric acid solution and 3 g ferric chloride) to reveal the microstructure. Microstructural examination of the specimens was carried out using standard optical microscopy and scanning electron microscopy. The phase compositions of these specimens that were not etched after polishing were analyzed using a X-ray diffractometer.

The electrochemical corrosion test was carried out by using the Preceton-Versa STAT3 electrochemistry workstation. The software in the electrochemical workstation can automatically measure the electrochemical corrosion. It included potential dynamic polarization, corrosion potential measurement, Tafel curve fitting and AC impedance testing. The data fitting analysis of AC impedance was completed by zsimpwin software. The conventional three electrode electrochemical corrosion test cell was used for electrochemical corrosion test. The working electrode, counter electrode and reference electrode are inserted into the test unit, and the maximum solution volume of the cell was 100 ml. The sample to be tested was $10 \times 10 \times 5$ mm welding overlays. The electrochemical test solution was 3.5 wt.% NaCl + 0.01 mol/l HCl, the reference electrode is mercurous sulfate electrode, and the counter electrode was $15 \times 15 \times 0.3$ mm platinum plate. The scanning rate of polarization curve was 0.5 mv/s, and the scanning range was -0.4 V ~ 1.5 V vs. OCP in acidic solution. The AC impedance test parameters ranged from 0.01 Hz to 100 000 Hz.

3. Results and discussion

Fig. 2 shows XRD analysis of self-shielded metal-cored arc welding overlays with different niobium additions. It can be seen that the microstructure of niobium-containing welding overlays is composed of $(Cr, Fe)_7C_3$, $(Cr, Fe)_3C$, NbC carbides, martensite and austenite. With the increase of the addition of niobium, the diffraction peak of NbC is increased gradually, which indicates that the content of NbC is increased.

Fig. 3 shows the OM micrograph of self-shielded metal-cored arc welding overlays with different niobium additions. With the increase of the addition of niobium, the size of primary $M_7(C, B)_3$ carbide in the microstructure of the welding overlay is decreased, but the gray black NbC phase is increased. Moreover, the microstructure of the welding overlay becomes finer. It is difficult to find the primary $M_7(C, B)_3$ carbide when the addition of niobium is 10.8 wt.%. The microstructure of the overlay is mainly composed of NbC and eutectic structure, and NbC has a large-scale quadrilateral structure. Since the addition of niobium is further increased to 14.4 wt.%, dendritic hypoeutectic austenite is precipitated and NbC is distributed continuously and intensively. The microstructure of the welding overlay has changed from eutectic to hypoeutectic. Hence,
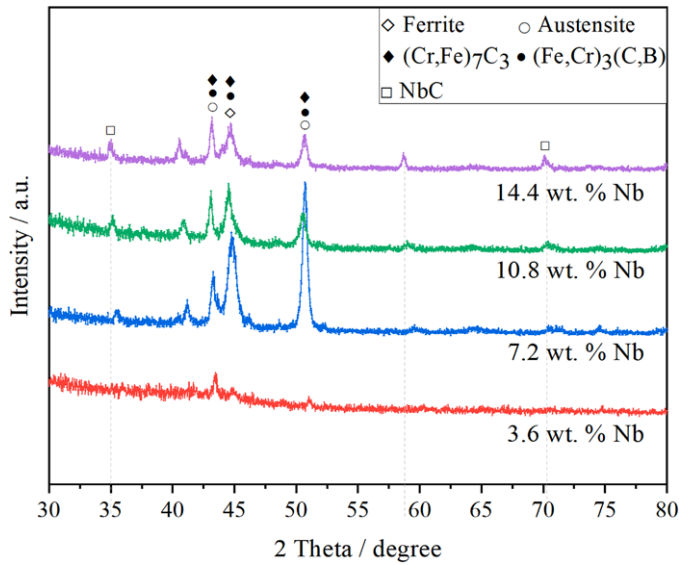
Fig. 2. XRD analysis of self-shielded metal-cored arc welding overlays with different niobium additions

with the increase of the addition of niobium addition in metal-cored wire, the microstructure of the welding overlay gradually changes from hypereutectic to eutectic and hypoeutectic, and the microstructure is refined continuously.

The affinity of niobium for carbon is so great that niobium may easily combine with carbon to form niobium carbides [18]. In hypereutectic high chromium welding overlay, NbC carbides are formed firstly, and then the $M_7(C, B)_3$ carbides are formed around the NbC precipitates. Since the formation of NbC is an enrichment of Cr and C between the NbC and the matrix, the rapid cooling after welding offers propitious conditions for the nucleus formation of chromium carbide. Thus, NbC can be used as carbide heterogeneous nuclei, which refines the primary $M_7(C, B)_3$ carbides. On the other hand, the consuming of carbon to form NbC, leading to the change of the microstructure of the welding overlay. Similar microstructure evolution was found in Ti doped hardfacing alloy owing to the formation of TiC which consumed carbon [20].

Fig. 4 shows SEM micrograph of self-shielded metal-cored arc welding overlays with different niobium additions, which is in agreement with the results of Fig. 3. Moreover, the niobium is rich in the gray black NbC phase but not the other phase in the microstructure (Fig. 4e).

Fig. 5 shows the polarization curve of self-shielded metal-cored arc welding overlays with different niobium additions in 3.5 wt.% NaCl solution + 0.01 mol/L HCl solution. At the niobium addition of 3.6 wt.%, the polarization curve is at the highest position. With the increase of niobium addition in the
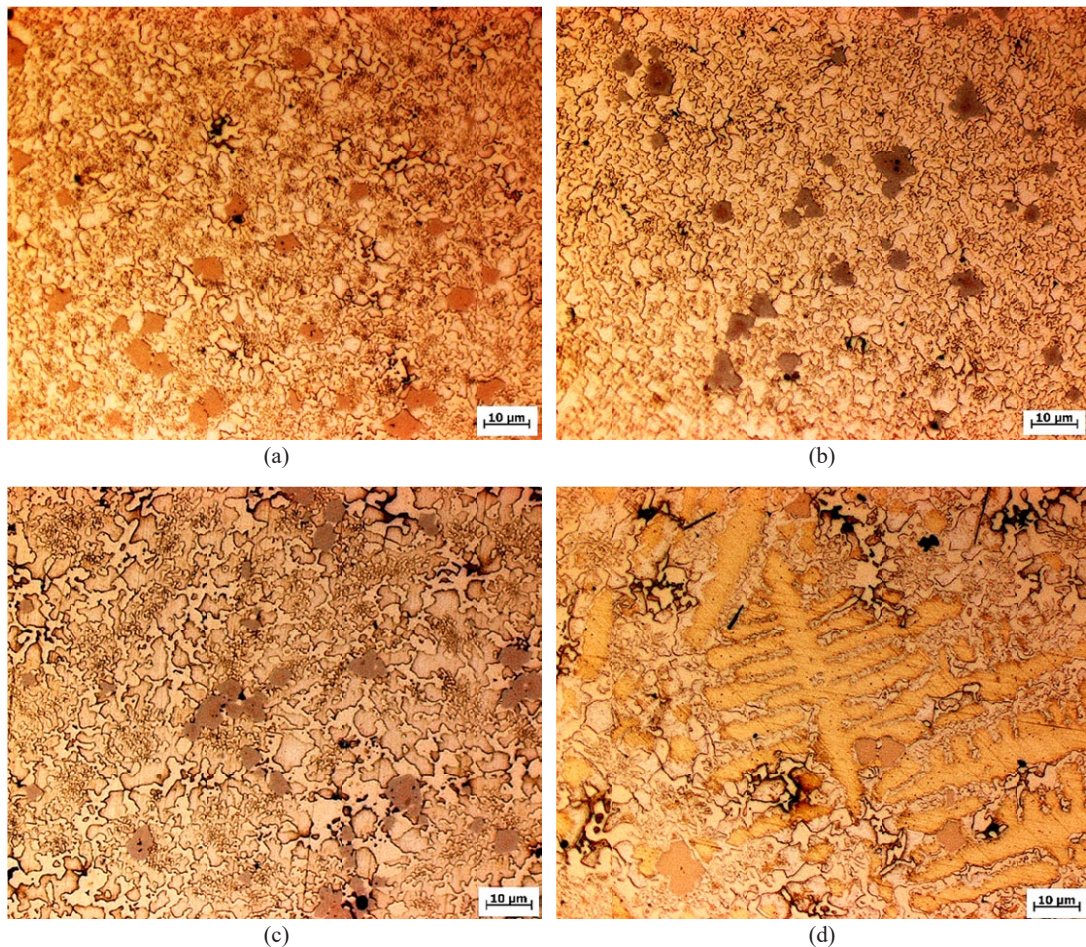

(a)

(b)

(c)

(d)

Fig. 3. OM micrograph of self-shielded metal-cored arc welding overlays with different niobium additions (a) 3.6 wt.% Nb, (b) 7.2 wt.% Nb, (c) 10.8 wt.% Nb, (d) 14.4 wt.% Nb
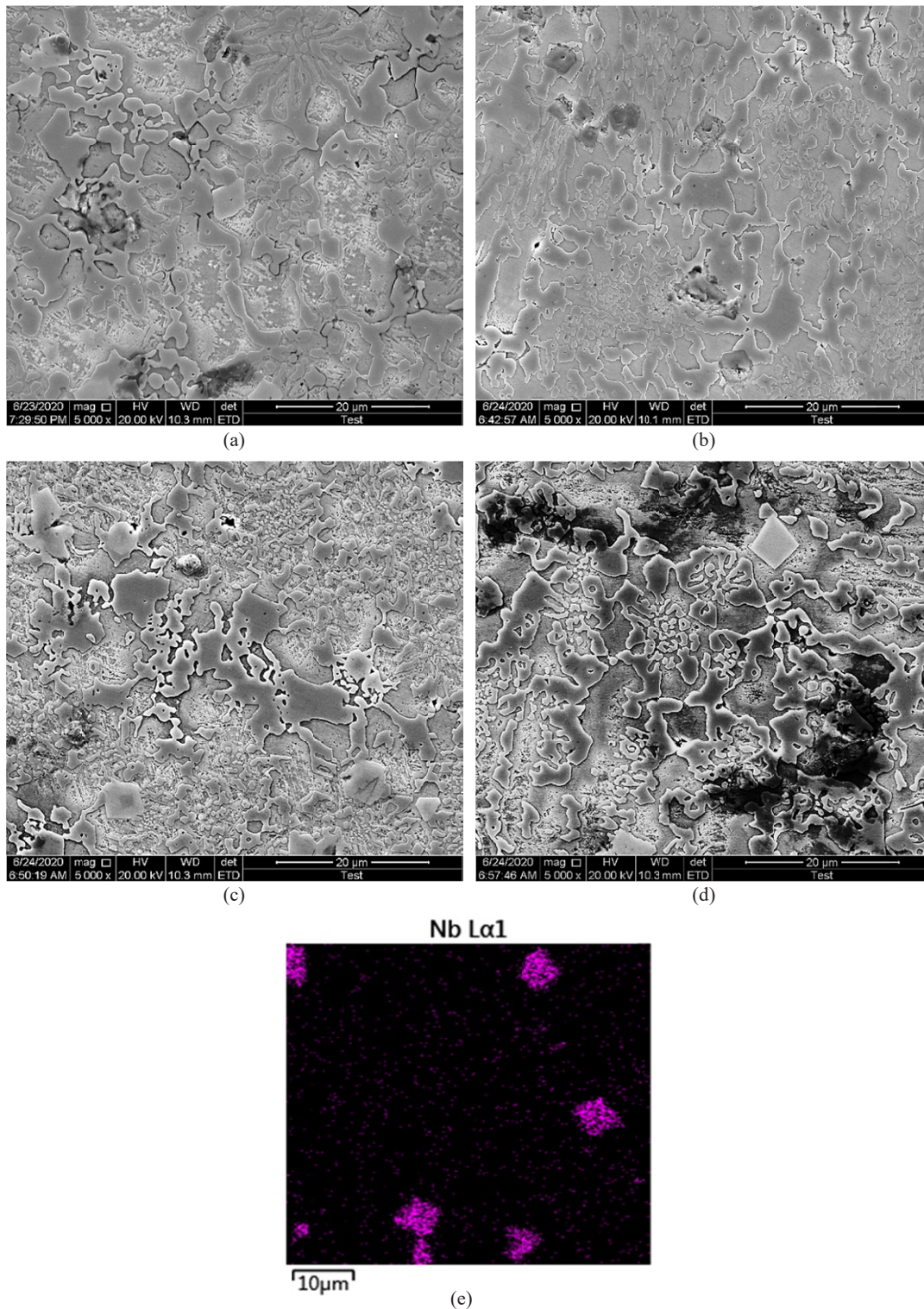
Fig. 4. SEM micrograph of self-shielded metal-cored arc welding overlays with different niobium additions (a) 3.6 wt.% Nb, (b) 7.2 wt.% Nb, (c) 10.8 wt.% Nb, (d) 14.4 wt.% Nb, (e) the distribution of Nb in Fig. 4(d)

welding wire, the polarization curve position is decreased firstly, and then increased. When the addition of niobium is 10.8 wt.%, the curve is in the lowest right area, the self-corrosion potential is at the lowest point, and the self-corrosion current increases sharply. Thus, the corrosion resistance is at the highest with 3.6 wt.% niobium addition, and at the lowest when the niobium addition is 10.8 wt.%.

Fig. 6 shows I_{corr} and E_{corr} of self-shielded metal-cored arc welding overlays with different niobium additions. When the addition of niobium is 3.6 wt.%, the self-corrosion potential E_{corr} is at the highest value of –0.956 V, and I_{corr} is at the minimum value of 2.53 A/cm^2, and the corrosion resistance of the alloy is the best among all the overlays. However, the overlay with 10.8 wt.% niobium addition has the lowest self-corrosion potential E_{corr} of
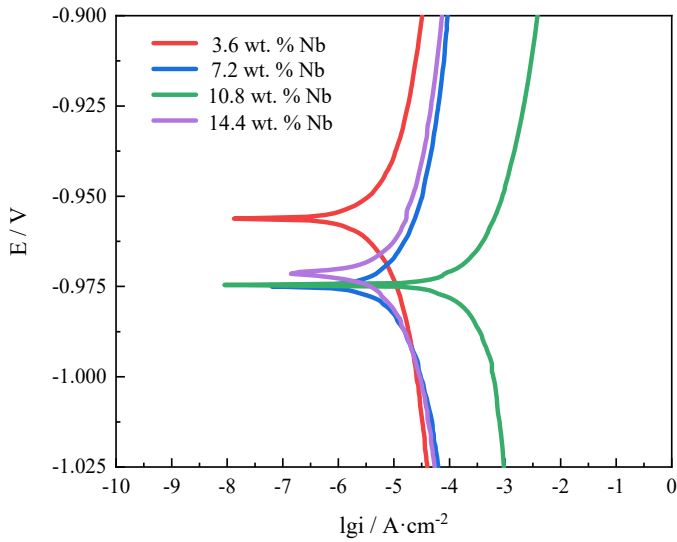
Fig. 5. Polarization curve of self-shielded metal-cored arc welding overlays with different niobium additions in 3.5 wt.% NaCl solution + 0.01 mol/L HCl solution

–0.975 V, and the maximum self-corrosion current density I_{corr} is 215.18×10^{-6} A / cm^2, which indicates that the surfacing alloy has the lowest corrosion resistance. It can be seen that with the increase of niobium addition, the corrosion resistance of the welding overlay is decreased as a whole.
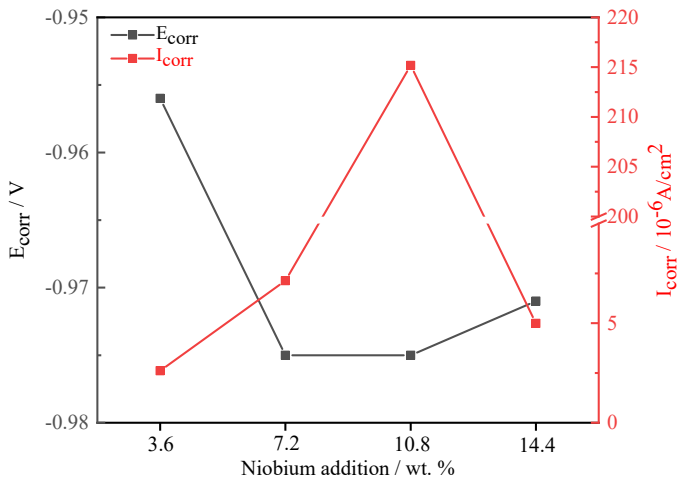

Fig. 6. I_{corr} and E_{corr} of self-shielded metal-cored arc welding overlays with different niobium additions

Fig. 7 shows Nyquist curve of welding overlays with different niobium additions. Fig. 8a exhibits equivalent circuit model for the impedance spectra measured in 3.5 wt.% NaCl solution + 0.01 mol/L HCl solution, which is available to the welding overlay with 0 wt.%, 3.6 wt.%, 7.2 wt.% and 14.4 wt.% niobium addition. However, the equivalent circuit model shown in Fig. 8b which belongs to concentration polarization corrosion electrode system applies only to the welding overlay with 10.8 wt.%.

TABLE 1 shows the values of the equivalent circuit elements for the impedance spectra measured in 3.5 wt.% NaCl + 0.01 mol/L HCl solution, and Fig. 9 summarizes their change
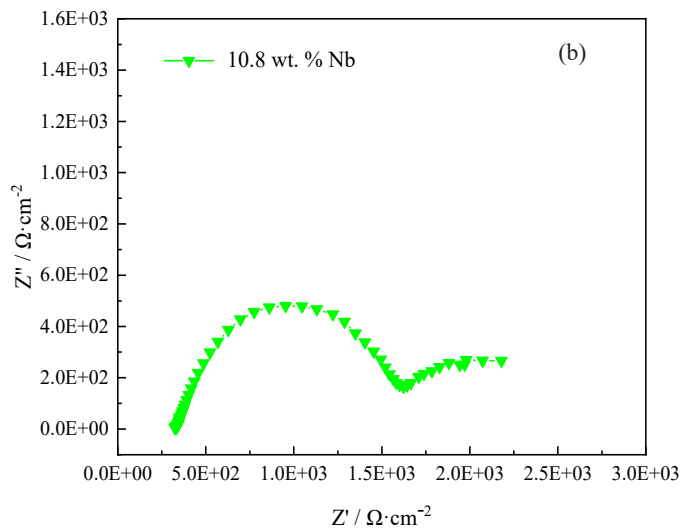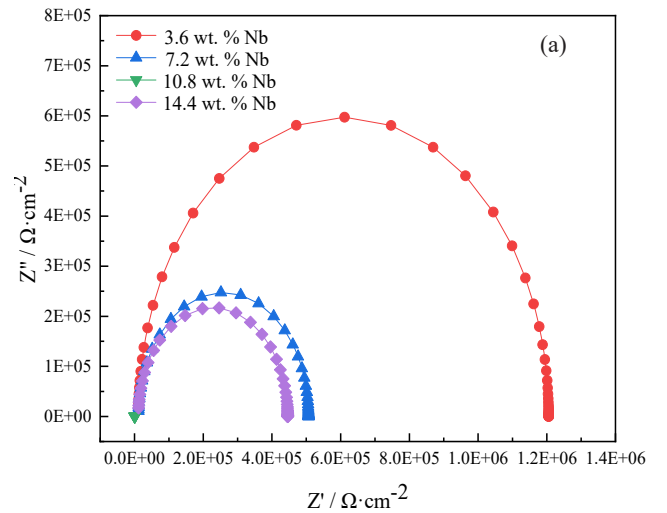

Fig. 7. Nyquist curve of welding overlays with different niobium addition in 3.5 wt.% NaCl solution + 0.01 mol/L HCl solution (a) 3.6 wt.% Nb, 7.2 wt.% Nb and 14.4 wt.% Nb, (b) 10.8 wt.% Nb
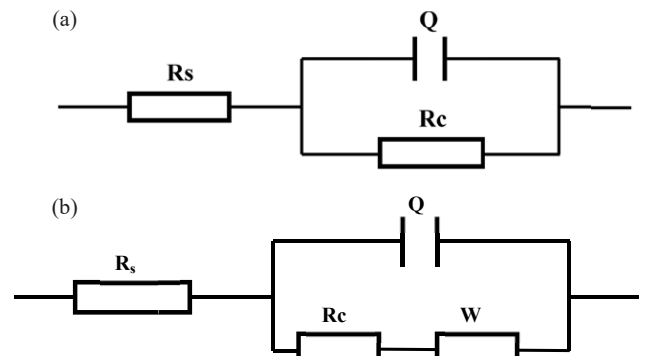

Fig. 8. Equivalent circuit model for the impedance spectra measured in 3.5 wt.% NaCl solution + 0.01 mol/L HCl solution (a) for 3.6 wt.% Nb, 7.2 wt.% Nb and 14.4 wt.% Nb, (b) for 10.8 wt.% Nb

trend of R_c values. It can be seen that when the niobium addition is 3.6 wt.%, R_c exhibits maximum value of 1.194×10^6 $\Omega \cdot$cm^2. R_c is deceased to the minimum value (1216 $\Omega \cdot$cm^2) with the niobium addition increasing to 10.8 wt.%, which indicates a worst corrosion resistance.

Values of the equivalent circuit elements for the impedance spectra
measured in 3.5 wt.% NaCl solution

Additions of Nb (wt.%)	Equivalent circuit elements			
	R_s ($\Omega \cdot cm^2$)	Q ($\Omega \cdot cm^2$)	R_c ($\Omega \cdot cm^2$)	R_w ($\Omega \cdot cm^2$)
0	1.095×10^4	8.686×10^{-11}	6.878×10^5	—
3.6	1.125×10^4	1.121×10^{-10}	1.194×10^6	—
7.2	1.157×10^4	1.381×10^{-10}	4.950×10^5	—
10.8	3.589×10^2	3.859×10^{-6}	1.216×10^3	3.262×10^{-3}
14.4	1.102×10^1	8.788×10^{-11}	4.348×10^5	—

Fig. 10 shows OM micrograph of self-shielded metal-cored arc welding overlays with different niobium additions in 3.5 wt.% NaCl + 0.01 mol/L HCl solution. The corrosion of welding overlay occurs in the matrix of microstructure. With the increase of niobium addition from 3.6 wt.% to 10.8 wt.%, the proportion of network eutectic structure in the welding overlay is increased. Up to 10.8 wt.% of the welding overlay, the microstructure is completely transformed from hypereutectic structure into eutectic one. Although the content of NbC carbide in the overlay is increased with the increase of niobium addition, the proportion of eutectic structure is increased, and the network eutectic structure greatly increases the reaction interface in the corrosion process, which greatly speeds up the corrosion rate and thus reduces the corrosion resistance. The OM images also
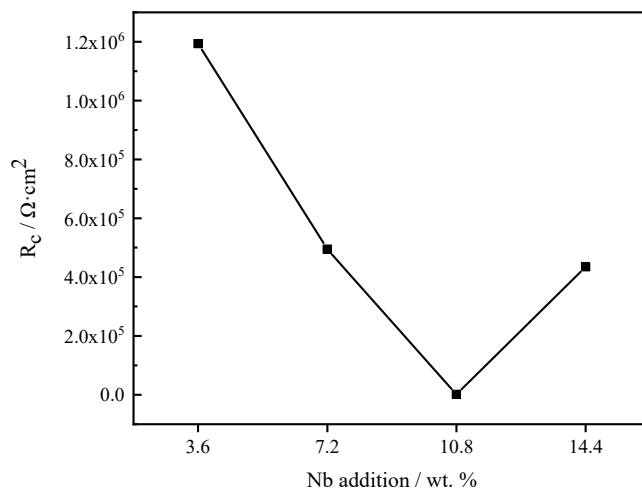

Fig. 9. Change trend of R_c values for welding overlays with different niobium additions

indicate that the corrosion resistance of the welding overlays is decreased continuously with the increase of niobium addition from 3.6 wt.% to 10.8 wt.% (Fig. 10a-c). When niobium addition reaches 14.4 wt.%, the welding overlay is transformed into a hypoeutectic structure. The addition of niobium element consumes carbon element in the alloy, which makes the increase of chromium content in the final solidified matrix, leading to an improvement in corrosion resistance. It can be seen from
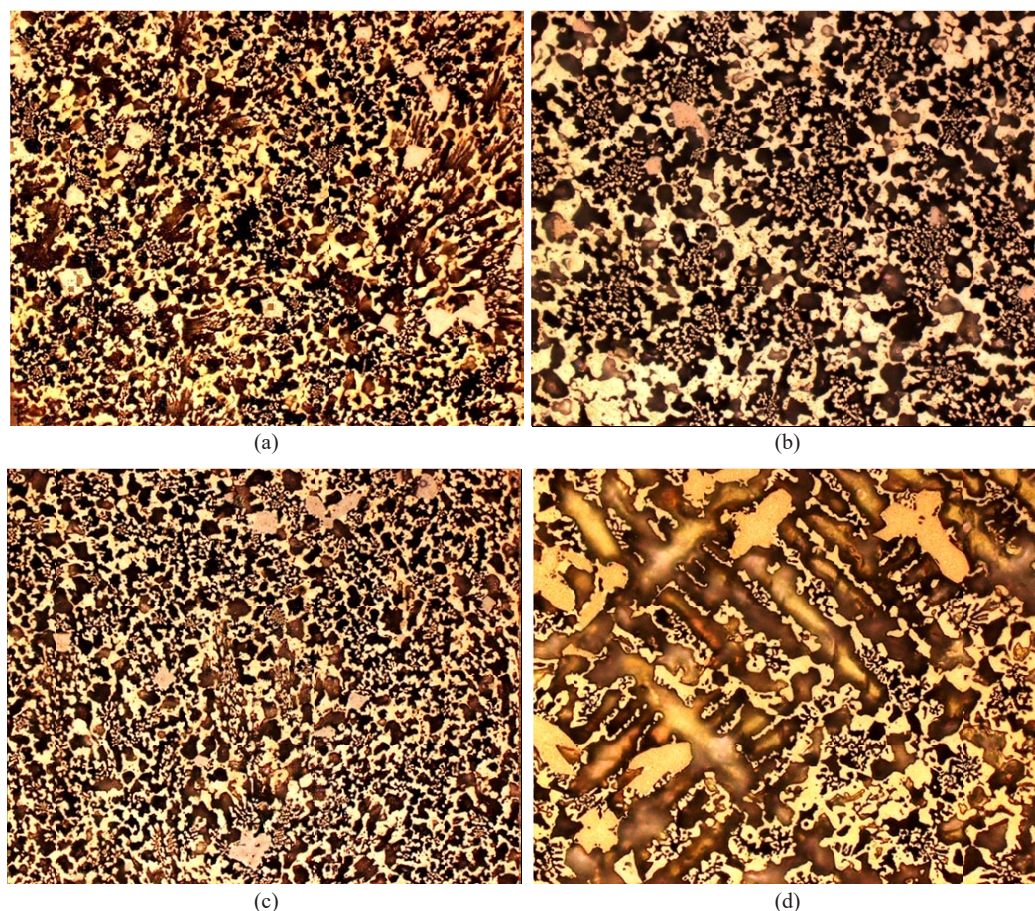

(a)

(b)

(c)

(d)

Fig. 10. OM micrograph of self-shielded metal-cored arc welding overlays with different niobium additions in 3.5 wt.% NaCl + 0.01 mol/L HCl solution (a) 3.6 wt.% Nb, (b) 7.2 wt.% Nb, (c) 10.8 wt.% Nb, (d) 14.4 wt.% Nb

Fig. 10d that the eutectoid austenite structure remains relatively intact after corrosion, which indicates that the corrosion resistance of the welding overlay is increased to a certain extent due to the addition of 14. 4 wt.% niobium.

Fig. 11 shows SEM micrograph of self-shielded metal-cored arc welding overlays with different niobium additions in 3.5 wt.% NaCl + 0.01 mol/L HCl solution. In accordance with the results of OM observation, the corrosion reaction in Fig. 11a-c is increased with the increasing proportion of eutectic structure. In Fig. 11c, except that the surface of NbC and eutectic carbide is in good condition, the network corrosion pits are formed in eutectic structure matrix due to severe corrosion reaction. When the addition of niobium is increased to 14.4 wt.%, the depth of corrosion pit formed after corrosion is reduced compared with that in Fig. 11d due to the increase of chromium content in the matrix.

4. Conclusions

In this study, the high-Cr iron-based alloys with different niobium addition were fabricated by using self-made self-shielded metal-cored wires and their microstructure and acidic

corrosion resistance in 3.5 wt.% NaCl solution + 0.01 mol/L HCl solution were investigated. From the results, the following conclusions can be drawn:

(1) At the niobium addition of 3.6 wt.%, the polarization curve is at the highest position. With the increase of niobium addition in the welding wire, the polarization curve position is decreased firstly, and then increased. When the addition of niobium is 10.8 wt.%, the curve is in the lowest right area, the self-corrosion potential is at the lowest point, and the self-corrosion current increases sharply. The values of I_{corr}, E_{corr} and R_c are in agreement with the polarization curves. Thus, the corrosion resistance is at the highest with 3.6 wt.% niobium addition, and at the lowest when the niobium addition is 10.8 wt.%.

(2) The corrosion of welding overlay occurs in the matrix of microstructure. With the increase of niobium addition from 3.6 wt.% to 10.8 wt.%, the proportion of network eutectic structure in the welding overlay is increased. Up to 10.8 wt.% of the welding overlay, the microstructure is completely transformed from hypereutectic structure into eutectic one. Although the content of NbC carbide in the overlay is increased with the increase of niobium addition, the proportion of eutectic structure is increased, and the
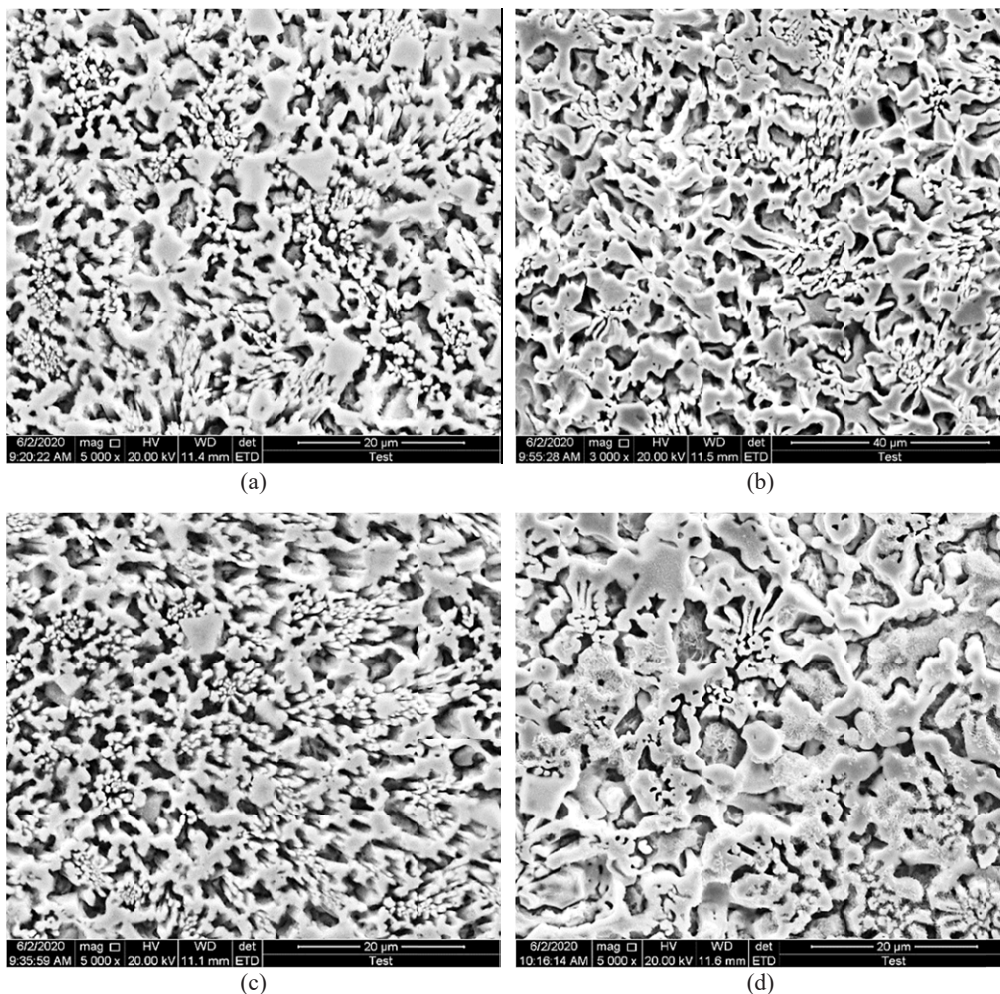

(a)

(b)

(c)

(d)

Fig. 11. SEM micrograph of self-shielded metal-cored arc welding overlays with different niobium additions in 3.5 wt.% NaCl + 0.01 mol/L HCl solution (a) 3.6 wt.% Nb, (b) 7.2 wt.% Nb, (c) 10.8 wt.% Nb, (d) 14.4 wt.% Nb

network eutectic structure greatly increases the reaction interface in the corrosion process, which greatly speeds up the corrosion rate and thus reduces the corrosion resistance. When niobium addition reaches 14.4 wt.%, the welding overlay is transformed into a hypoeutectic structure. The addition of niobium element consumes carbon element in the alloy, which makes the increase of chromium content in the final solidified matrix, leading to an improvement in corrosion resistance.

REFERENCES

[1] J. Pearce, T.H. Chairuangsri, T. Imurai, S. Thanachayanont Ch, Microstructure and erosion-corrosion behaviour of as-cast high chromium white irons containing molybdenum in aqueous sulfuric-acid slurry., Arch. Metall. Mater. **60** (2), 919-923 (2015).
DOI: https://doi.org/10.1515/amm-2015-0230

[2] J.T.H. Pearce, High-chromium cast irons to resist abrasive wear, Foundryman. **95**, 156-166 (2002).

[3] A.E. Karantzalis, A. Lekatou, H. Mavros, Microstructural modifications of as-cast high-chromium white iron by heat treatment, J. Mater. Eng. Perform. **18** (2), 174-181 (2009).
DOI: https://doi.org/10.1007/s11665-008-9285-6

[4] E. Zumelzu, I. Goyos, C. Cabezas, O. Opitz, A. Parada, Wear and corrosion behaviour of high-chromium (14-30% Cr) cast iron alloys, J. Mater. Process. Technol. **128** (1-3), 250-255 (2002).
DOI: https://doi.org/10.1016/S0924-0136(02)00458-2

[5] M.M. Lachowicz, M.B. Lachowicz, The mechanism of corrosion of steel 304L in the presence of copper in industrial installations, Arch. Metall. Mater. **60** (4), 2657-2662 (2015).
DOI: https://doi.org/10.1515/amm-2015-0429

[6] A. Smołka, G. Dercz, K. Rodak, B. Łosiewicz, Evaluation of corrosion resistance of nanotubular oxide layers on the Ti13Zr13Nb alloy in physiological saline solution, Arch. Metall. Mater. **60** (4), 2681-2686 (2015).
DOI: https://doi.org/10.1515/amm-2015-0432

[7] J.H. Lee, I.H. Oh, H.K. Park, Effects of transition metal carbides on microstructure and mechanical properties of ultrafine tungsten carbide via spark plasma sintering, Arch. Metall. Mater. **66** (4), 1029-1032 (2021).
DOI: https://doi.org/10.24425/amm.2021.136419

[8] H.H. Tian, G.R. Addie, R.J. Visintainer, Erosion-corrosion performance of high-Cr cast iron alloys in flowing liquid-solid slurries, Wear **267** (11), 2039-2047 (2009).
DOI: https://doi.org/10.1016/j.wear.2009.08.007

[9] K.A. El-Aziz, K. Zohdy, D. Saber, H.E.M. Sallam, Wear and corrosion behavior of high-Cr white cast iron alloys in different corrosive media., J. Bio. Tribo. Corros. **1**, 25 (2015).
DOI: https://doi.org/10.1007/s40735-015-0026-8

[10] X.H. Tang, R. Chung, D.Y. Li, B. Hinckley, K. Dolman, Variations in microstructure of high chromium cast irons and resultant changes in resistance to wear, corrosion and corrosive wear, Wear **267** (1), 116-121 (2009).
DOI: https://doi.org/10.1016/j.wear.2008.11.025

[11] A. Wiengmoon, J. Pearce, T. Chairuangsri, Relationship between microstructure, hardness and corrosion resistance in 20 wt.%Cr, 27 wt.%Cr and 36 wt.% Cr high chromium cast irons, Mater. Chem. Phys. **125** (3), 739-748 (2011).
DOI: https://doi.org/10.1016/j.matchemphys.2010.09.064

[12] J.F. Gou, Y. Wang, X.W. Li, Y.F. Zhou, Effect of rare earth oxide nano-additives on the corrosion behavior of Fe-based hardfacing alloys in acid, near-neutral and alkaline 3.5 wt.% NaCl solutions, Appl. Surf. Sci. **431**, 143-151 (2017).
DOI: https://doi.org/10.1016/j.apsusc.2017.06.203

[13] G. Karafyllias, A. Galloway, E. Humphries, The Effect of low pH in erosion-corrosion resistance of high chromium cast irons and stainless steels, Wear **420-421**, 79-86 (2019).
DOI: https://doi.org/10.1016/j.wear.2018.11.021

[14] K.Y. Lee, S.H. Lee, Y. Kim, H.S. Hong, Y.M. Oh, S.J. Kim, The effects of additive elements on the sliding wear behavior of Fe-base hardfacing alloys, Wear **255** (1-6), 481-488 (2003).
DOI: https://doi.org/10.1016/S0043-1648(03)00155-8

[15] Q. Wang, X. Li, Effects of Nb, V, and W on microstructure and abrasion resistance of Fe-Cr-C hardfacing alloys, Int. J. Sport Exer. Ps. **5** (2), 256-258 (2010).
DOI: https://doi.org/10.1080/1612197X.2007.9671827

[16] G.C. Coelho, J.A. Golczewski, H.F. Fischmeister, Thermodynamic calculations for Nb-containing high-speed steels and white-cast-iron alloys, Metall. Mater. Trans. A **34** (9), 1749-1758 (2003).
DOI: https://doi.org/10.1007/s11661-003-0141-x

[17] Q. Li, Y. Zhang, Y. Zhang, H. Liu, H. Ren, Y. Zhong, X.F. Huang, W. Huang, Influence of Sn and Nb additions on the microstructure and wear characteristics of a gray cast iron, Appl. Phys. A. Solids. Surf. **126**, 282 (2020).
DOI: https://doi.org/10.1007/s00339-020-03468-8

[18] A. Cruz-Crespo, R. Fernández-Fuentes, A.V. Ferraressi, R.A. Gonçalves, A. Scotti, Microstructure and abrasion resistance of Fe-Cr-C and Fe-Cr-C-Nb hardfacing alloys deposited by S-FCAW and cold solid wires, Rev. Soldagem. Inspecao. **21** (3), 342-353 (2016).
DOI: https://doi.org/10.1590/0104-9224/SI2103.09

[19] F. Sadeghi, H. Najafi, A. Abbasi, The effect of Ta substitution for Nb on the microstructure and wear resistance of an Fe-Cr-C hardfacing alloy, Surf. Coat. Technol. **324**, 85-91 (2017).
DOI: https://doi.org/10.1016/j.surfcoat.2017.05.067

[20] D.S. Liu, R.P. Liu, Y.H. Wei. Effect of titanium additive on microstructure and wear performance of iron-based slag-free self-shielded flux-cored wire, Surf. Coat. Technol. **207**, 579-586 (2012).
DOI: https://doi.org/10.1016/j.surfcoat.2012.07.078